Original Article [CNSJ]

A hydrodynamical study to propose a numerical index for evaluating the CSF conditions in cerebral ventricular system

Seifollah Gholampour, PhD[1]; Nasser Fatouraee, PhD[2]; Amir Saied Seddighi, MD[3]; Saeed Oraee Yazdani, MD[3]

[1] Department of BioMedical Engineering, Science and Research Branch, Islamic Azad University
[2] Biological Fluid Laboratory, Biomedical Engineering Faculty, Amirkabir University of Technology, Tehran, Iran
[3] Functional Neurosurgery Research Center, Shohada Tajrish Hospital, Shahid Beheshti University of Medical Sciences, Tehran, Iran

ABSTRACT

Background: CSF is a clear liquid that its mechanical properties are to a large extent similar to water properties. Regarding the lack of a numerical index for diagnosis of diseases resulting from increased CSF pressure such as hydrocephalus, evaluation of hydrodynamic conditions of CSF in cerebral ventricular system is of great importance.
Methods: At first, the diagram of velocity in Sylvius aqueduct which was obtained through a 3D FSI analysis in ADINA was compared to the similar diagram extracted from CINE-PC-MRI of the same test subject. The next step after ensuring that the two diagrams coincide with each other, was to make sure that the problem assumptions and solution are correct. Thereafter, the Womersley number in Sylvius aqueduct of a healthy subject was calculated.
Results: The amount of this number was 3.25 and indicated the pulsatility of the fluid flow. The difference between the maximum and minimum pressure exerted by CSF on the brain tissue in Sylvius aqueduct was 81.5 Pa. This pressure difference was introduced for the first time in this study as an index for assessing hydrocephalus. Finally, the CSF pressure values calculated in this study and the pressure data obtained from LP test were compared.
Conclusion: This comparison showed that utilizing a proper pressure gauge for LP test makes it possible to use the LP test results, alongside with the study results, as an index to assess the CSF conditions in ventricular system for diagnosis of that group of diseases resulting from increase in CSF pressure.

Keywords: Cerebrospinal fluid; Pressure; Lumbar puncture; Hydrocephalus

ICNSJ 2014; 1 (1) :1-9 http://journals.sbmu.ac.ir/neuroscience

Correspondence to: Amir Saied Seddighi, MD; Functional Neurosurgery Research Center, Shohada Tajrish Hospital, Tajrish Sq, Tehran, Iran; E-mail: A_sedighi@sbmu.ac.ir; Tel: +98(91)22151591
Received: May 7, 2014 **Accepted:** August 3, 2014

INTRODUCTION

Cerebrospinal fluid (CSF) is a clear and colorless liquid produced in the choroid plexus of brain ventricles and circulates in the ventricular system, cisterna magna and subarachnoid space. The composition of CSF is similar to that of blood plasma but the concentration of its constituents differs from that in plasma[1]. Fluid mechanical properties of CSF, as seen in table 1, are to a large extent similar to water properties. The density in red zones of figure 1 indicates the greatest amount of CSF production which is related to lateral ventricles and to some extent to fourth ventricle (Ventriculus quartus).

Sodium and chlorine ions increase the amount of osmotically active substances in CSF and cause nearly immediate osmosis of water through the membrane of choroid plexus and consequently production and secretion of CSF. Part of the CSF, after circulation in its flow path, enters into sagittal sinus vein through arachnoid villi and is reabsorbed there into the blood circulation system[2-4]. Occlusion of cerebrospinal fluid path increases

Table 1. The assumptions for the fluid model (CSF)

Kinematic Viscosity (m^2/s)	density Kg/m^3)
0.000001004	998.2

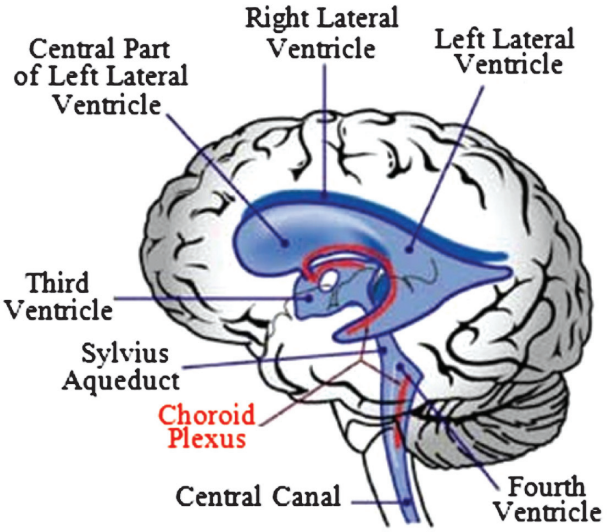

Figure 1. A view of ventricular system and brain tissue. The production sites and circulation paths of CSF have been shown by red and blue lines, respectively.

the pressure exerted by the liquid on the walls of the ventricles and ultimately leads to hydrocephalus.

Since fluid loading is exerted on the brain tissue making the walls of the flow path, the biomechanical properties of brain tissue significantly affect the disease conditions.

We take, therefore, the review of previous studies leading to a better understanding of biomechanical properties of brain tissue under various loadings as the starting point. Nagashima et al, produced a 2D brain image through computed tomography (CT) scanning and found the stress distribution and the resulted deformations in brain tissue using the finite elements method (FEM); the brain tissue was considered as a linearly elastic material for the first time in this study[5]. Continuing that research course, Miller et al, extracted the in-vitro biomechanical parameters of brain tissue by considering it as a hyper-viscoelastic material for the first time[6]. Liu completed those researches later and published a comprehensive theoretical analysis of hyper-viscoelastic relations and properties of brain tissue[7].

Finally, Chafi et al, carried out some studies to compare the dynamic responses of brain tissue under similar loading conditions and various assumptions of viscoelasticity, hyper-viscoelasticity and poroelasticity of tissue. They suggested frequency indices for this comparison using 2D FEM and also explored the mutual effect of CSF and brain tissue under external loading[8].

Most of those researches, however, failed to study the brain tissue under CSF loading from the viewpoint of fluid mechanics. Taylor et al, considered the brain tissue as a linearly elastic material and investigated a 2D section of lateral ventricles of two samples using FEM and assessed the effect of the brain tissue module of elasticity on brain deformations in healthy and diseased samples[9]. Other studies have been also carried out to measure the velocity and flow rate of CSF and to evaluate the effect of pressure on the wall of ventricles[8,9]. These studies investigated the CSF velocity, flow rate and pressure mainly in certain anatomical crosssections like Sylvius aqueduct or Monro foramen and in two dimensions. Although much effort has been devoted to reconstruction of the CSF flow in two dimensions[10], a 2D approach has the disadvantage of not rendering the volume relationships accurately. For instance, while considering only a 2D cross section along the longitudinal fissure of the brain, either the cerebral ventricles are missed completely or the space between the two hemispheres isn't rendered correctly. Moreover, the spatial relationship between the pontine cistern and the ventricular space can't be properly rendered by a 2D model, and thus, more advanced models of aqueduct are needed to study its deformability[11].

As known, a 2D analysis of a certain section of ventricular system cannot render the exact effect of interaction between CSF and brain tissue due to geometrical complexities of ventricles; hence, another group of studies performed a 3D analysis of flow in ventricles. However, they studied just a part of the ventricular system, for instance the third ventricle, through 3D models. The results of these researches had, therefore, serious deficiencies due to not rendering all the complexities of ventricular system and their effects on fluid mechanical components of flow. Many of these studies explored the CSF flow outside the ventricular system, for example in subarachnoid space or in cisterns, and used the ventricular system in the boundary conditions of the relevant problems[12,13].

Jacobson et al, explored the CSF pressure in a stenosis in the path of ventricular system using a 3D model and computational fluid dynamics (CFD) method[14,15]. Linge et al, proposed a 3D model of the lower part of subarachnoid space and the spinal cord of cervical area and analyzed the fluid mechanical parameters of flow in those regions[16]. Gupta et al, analyzed the hydrodynamics of CSF in intracranial space and subarachnoid space[17]. Most of these studies, however, used CFD approach to analyze

the flow in two and three dimensions. CFD analysis has deficiencies in comparison to Fluid-structure interaction (FSI) analysis, which analyzes the interaction of fluid and solid models simultaneously, and its results correspond to a lesser extent with the real conditions of the walls of brain ventricles under the load of CSF.

Another group of researches were only laboratory studies with the aim of suggesting the CSF velocity and flow rate data extracted from phase contrast magnetic resonance imaging (PC-MRI) as evaluating indices of CSF conditions in brain ventricles. Examining the maximum flow rate and velocity as statistical monitoring indices of exerted pressure by CSF on ventricular walls and presenting tables and graphs to compare the CSF conditions in individuals of various age and gender were deemed important in those researches[18,19]. Zhu et al, investigated the CSF velocity in lateral ventricles using cine phase contrast magnetic resonance imaging (CINE-PC-MRI) and presented the statistical relations between the size change and CSF flow in ventricles of healthy and hydrocephalic samples[20]. No biofluid mechanical analysis, however, was done in this group of studies and no reliable index was proposed for diagnostic purposes. The deformation of ventricles due to increase or decrease in CSF pressure was also not explored.

Sweetman et al, carried out a study on the CSF pressure difference in subarachnoid space and ventricular system. Using FSI and 3D modeling of flow, they introduced the aforementioned pressure difference as an index to compare the conditions between healthy and communicating hydrocephalic samples[21]. In the present study, the diagram of CSF velocity in various cross sections of ventricular system has been calculated using FSI method and the velocity, pressure and deformation outputs have been presented. Moreover, the difference between minimum and maximum CSF pressure exerted on the brain tissue has been analyzed and evaluated as an index of CSF conditions in ventricular system.

METHODS AND MATERIAL

First, a CINE-PC-MRI of the head of a 36-year-old woman was produced. Detailed flow results and data acquisition methods were described previously[21,22]. The first obtained output based on the cardiac cycle was the diagram of CSF velocity in Sylvius aqueduct which was merely used to control and validate the correctness of responses and had no application in problem solving process. The second output was DICOM file of the subject head. This file was transferred to the Mimics v12.11 for extraction of point cloud. Thereafter, the produced point cloud of the outer surfaces of ventricular system and brain tissue was inputted into the CATIA v5.R21. After building the 3D models of ventricular system and brain tissue, the models were transferred to ADINA-FSI 7.4 for meshing. Figure 2 shows the point cloud and the 3D model of the ventricular system.

Figure 3 and 4 show the 3D models of brain tissue and ventricular system after meshing by ADINA software. The assumptions for fluid and solid models, according to tables 1 and 2, were applied to ventricular system (fluid model) and brain tissue (solid model) following the meshing phase[21]. The tetrahedral element was used in this problem. In the end, the FSI results were calculated by ADINA. Following the extraction of outputs, the diagram

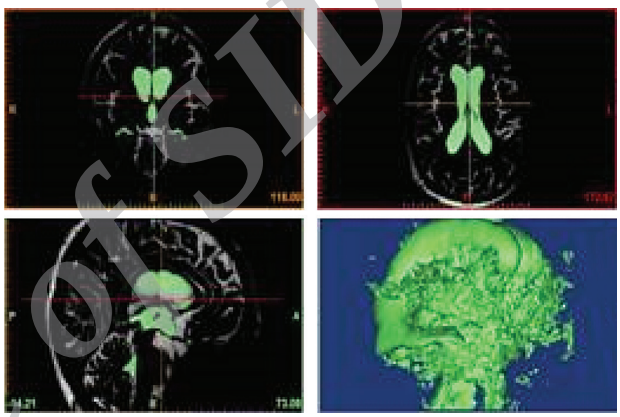

Figure 2. Manual segmentation of the CSF-filled spaces of the ventricular system resulted in the initially crude surface shown in the picture.

Figure 3. Views of the meshed model of ventricular system (fluid model) obtained from the ADINA software.

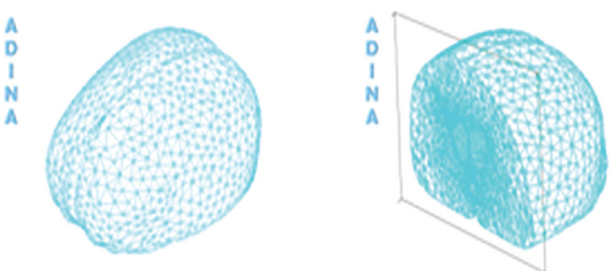

Figure 4. Views of the meshed model of brain tissue (solid model) obtained from the ADINA software.

Table 2. The assumptions for the solid model (brain tissue)

Young's modulus (KPa)	Shear modulus (KPa)	Poisson ratio
10	3.4	0.45

of the calculated velocity by ADINA in Sylvius aqueduct was compared with that of the velocity extracted from the CINE-PC-MRI of the subject's head and after ensuring the agreement between the data obtained from software and the experimental data and verifying the rightness of solution, the other results were analyzed.

FLUID–SOLID BOUNDARY CONDITIONS

The input flow rate is 0.5 ml/min and the movement pattern of this flow matches the oscillating function of blood in basilar artery[23]. Therefore to obtain the function of the input flow rate, the diagram of blood flow rate in basilar artery was first normalized based on the cardiac cycle[21] and then the normalized blood flow rate and the constant amount of 0.5 ml/min, which is the numerical amount of CSF flow rate in ventricular system according to physiologic data[2], were superposed using MATLAB 7.7. The result of superposition is the input flow rate function seen in figure 5. The lateral ventricles were considered based on physiologic data as the input location of flow[2]. The final section of the fourth ventricle was assumed as the output location of flow and the pressure of the output flow was considered 516 MPa according to physiologic data[2].

Brain tissue is the solid model and CSF is the fluid model. The deformations of the outer surfaces of the solid model were ignored and the outer surfaces of the brain tissue were constrained along the three directions of principle axes. In this study, the brain tissue was considered, based on similar assumptions as in other studies, as a linearly elastic material with the module of elasticity of 10 kPa[9],24. Regarding the use of FSI approach and ALE equations for simultaneous analysis of the equations governing the solid and fluid model, the governing equations are as follows:

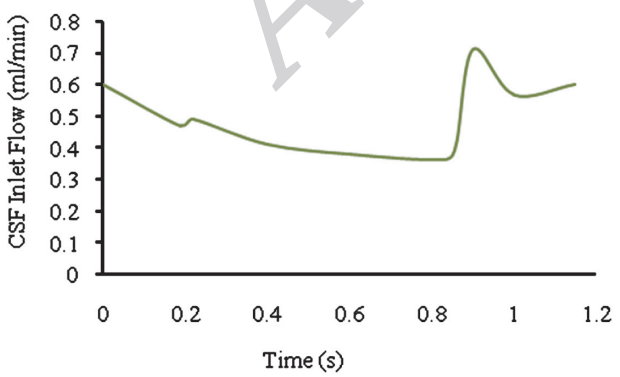

Figure 5. The result of superposition of the normalized function of blood flow rate and the constant value of 0.5 ml/min (amount of CSF flow rate) which is applied as the CSF flow rate function based on the cardiac cycle to input conditions.

The solid model was formulated using the Lagrangian model:

$$\frac{\partial \tau_{ij}^{s}}{\partial x_j} = \rho^{s} \frac{\partial^2 d_i^{s}}{\partial t^2} \quad (1)$$

where, ρ^s, d^s and $\tau_{ij}{}^s$ are the density, boundary displacement and Cauchy's stress tensor in solid part, respectively[25].

CSF was defined as an isothermal incompressible Newtonian fluid and the flow was considered as a laminar flow under the equations of conservation of mass and momentum as follows:

$$\frac{1}{\beta}\frac{\partial p}{\partial t} + \frac{\partial u_i}{\partial x_i} = 0 \quad (2)$$

$$\rho^{f}\frac{\partial u_i}{\partial t} + \rho^{f}\left(u_j - \frac{\partial d_j^{f}}{\partial t}\right)\frac{\partial u_i}{\partial x_j} = \frac{\partial \tau_{ij}^{f}}{\partial x_j} \quad (3)$$

where, β is the bulk coefficient, P the pressure of CSF, u_i the velocity of CSF in direction i, ρ^f the density of CSF and d^f the displacement of fluid model.

The Cauchy's stress tensor of fluid model τ_{ij}^{f} can be defined as follows:

$$\tau_{ij}^{f} = -p\delta_{ij} + 2\mu e_{ij} \quad (4)$$

where, δ_{ij} is the Kronecker delta and μ the CSF viscosity.

The strain tensor e_{ij} can be also defined as follows:

$$e_{ij} = \frac{1}{2}\left(\frac{\partial u_i}{\partial x_j} + \frac{\partial u_j}{\partial x_i}\right) \quad (5)$$

u_i and u_j are the components of fluid velocity in directions i and j[25].

MESH CONDITIONS AND INDEPENDENCY

A tetrahedral mesh was selected for meshing the solid and fluid models. The number of elements for fluid and solid models were 595200 and 1652100 elements, respectively. The time step of solution was set to 0.01 sec.

The conditions of mesh independency were compared in four states for maximum velocity of fluid in Sylvius aqueduct. As seen in table 3, the difference between the maximum fluid velocities in Sylvius aqueduct decreases intensely with the increase in element numbers. The diagram of figure 6 shows the convergence of responses.

Table 3. The maximum fluid velocity in Sylvius aqueduct in terms of element numbers

Number of elements	Maximum velocity in sylvius aqueduct (cm/s)
468300	10.65
595200	9.92
742000	9.53
852100	9.49

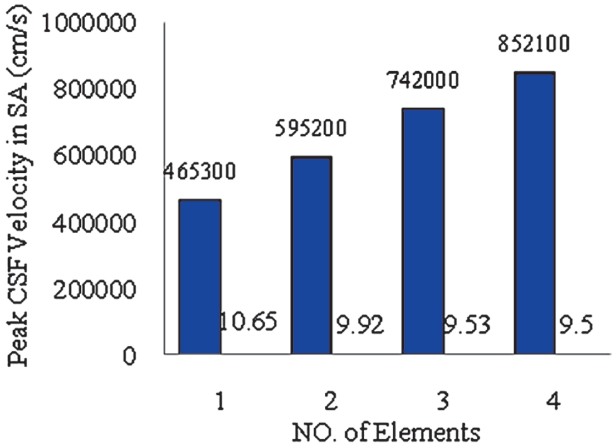

Figure 6. The diagram of maximum fluid velocity in Sylvius aqueduct in terms of element numbers. The convergence of responses and thus, their independency of mesh conditions can be seen.

RESULTS AND DISCUSSION

First, to ensure that the solution and assumptions made in this problem are correct, the function of CSF velocity in Sylvius aqueduct was calculated by the software and then compared to the velocity function extracted from the CINE-PC-MRI of the subject's head in the same cross section. After making sure that the analysis process is correct, the results of the functions of CSF velocity, pressure exerted by CSF on the ventricular system walls, and wall deformations in Sylvius aqueduct were extracted.

All results were extracted for four working cycles in periodic state by ADINA software and as no obvious difference was observed between the data of these cycles, the results of the last cycle were displayed for examination.

As shown in figure 7, the maximum and minimum velocity of CSF in Sylvius aqueduct were respectively 9.92 cm/s and -7.26 cm/s based on the data obtained from software and 10.43 cm/s and -7.42 cm/s based on the data extracted from CINE-PC-MRI of the subject's head.

The results show that the maximum and the minimum velocities in both diagrams coincide with each other with an error of less than 5% and the frequencies of velocity function in both diagrams have a desirable conformity which is deemed as a very positive point.

Considering the continuity relation and since the Sylvius aqueduct has the smallest cross-sectional area in the ventricular system, the CSF velocity in this section should be maximum and consequently, the amount of velocity should decrease with the increase in cross-sectional area as CSF moves towards the lateral ventricles. Figure 8 shows this trend of velocity reduction very well.

The velocity distribution at two different phases of the cardiac cycle has been compared in figure 9 and as expected, due to similarity of frequencies of the blood velocity function in basilar artery and CSF velocity

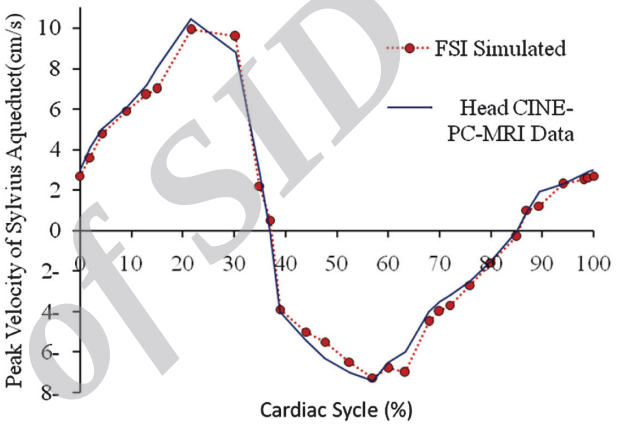

Figure 7. The comparison of CSF velocity diagrams in Sylvius aqueduct which were calculated by ADINA (red circles). The red circles show that the maximum CSF velocity in Sylvius aqueduct is 9.92 cm/s and its minimum velocity is -7.26 cm/s. The blue solid line shows that the maximum CSF velocity in Sylvius aqueduct is 10.43 cm/s and its minimum value is-7.42 cm/s.

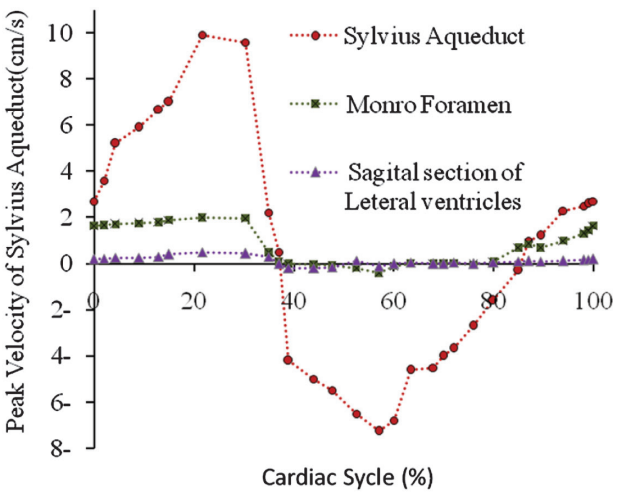

Figure 8. The comparison of diagrams of CSF velocity calculated based on cardiac cycle by ADINA in three cross sections. The red circle indicates the CSF velocity in Sylvius aqueduct and the green square shows the velocity in the Monro foramen and finally, the diagram of CSF velocity based on the cardiac cycle in the sagittal section of the lateral ventricles is shown by the violet triangle.

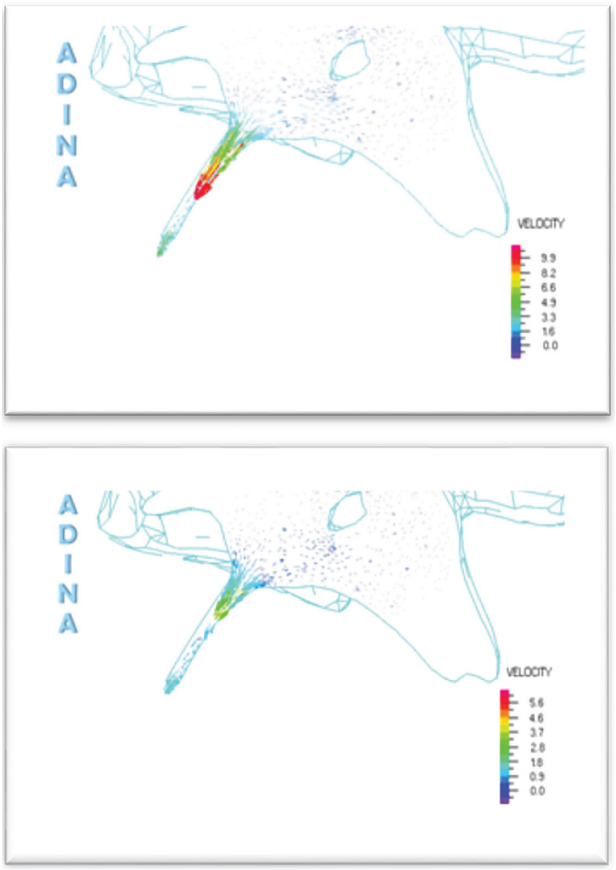

Figure 9. The distribution of CSF velocity (in cm/s) at the beginning of third ventricle. The top graph shows the fluid velocity distribution during the phase of mid systole at 15%of the cardiac cycle; the fluid has a relatively high velocity in this phase. The bottom graph shows the velocity distribution during the phase of diastole at 65% of the cardiac cycle; the fluid has a relatively low velocity in this phase.

function during the cardiac cycle[21], the maximum velocity of CSF in the cardiac cycle was seen in the mid systole phase (at 15% of cardiac cycle), in which the final stroke volume of CSF enters ventricular system. On the contrary, the fluid has a very low velocity in diastole phase at 65% of the cardiac cycle. Figure 10 and 11 shows the distribution and amount of pressure exerted on the brain tissue wall; the maximum value of this pressure is 616.3 Pa.

Analysis of CSF flow conditions

The present section is dedicated to description of fluid flow conditions which requires the study of Reynolds number in Sylvius aqueduct. Since the maximum velocity of the fluid and the radius of Sylvius aqueduct are 9.92 cm/s and 1.39 mm, respectively, the maximum value of Reynolds number is 275.7. The low Reynolds number indicates arelatively laminar flow which has been also confirmed by previous studies[26,22] and hence, the

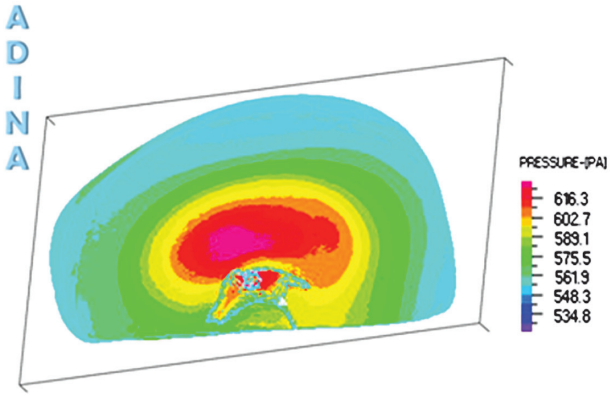

Figure 10. The distribution of CSF pressure on the walls of brain tissue.

equations of laminar flow can be used for analysis of the

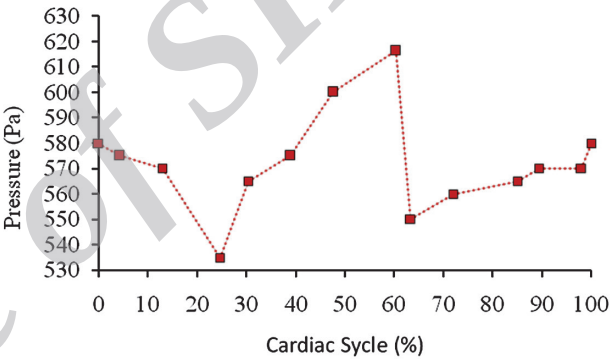

Figure 11. The pressure diagram in Sylvius aqueduct obtained from ADINA. The maximum and minimum pressure exerted by CSF on the brain tissue in Sylvius.

fluid conditions. It is also essential to present an analysis of the flow pulsatility level, of which the Womersley number is the best index. Solving the general form of Navier-Stokes equation and considering the Fourier series as the forcing function, the Womersley solution gives the number in Eq. (6) as the index of flow pulsatility.

$$\alpha = R\sqrt{\frac{\omega}{\nu}} \qquad (6)$$

Where, α is the Womersley number, ω the frequency of pressure function and ν the kinematic viscosity of fluid. R is the radius of aqueduct calculated from the Eq. (7).

$$R = \frac{A}{2\pi} \qquad (7)$$

Where, A is the cross-sectional area of Sylvius aqueduct. The period is 1.15 sec. according to the results of CINE-PC-MRI. The Womersley number for fluid flow equals 3.25 based on Eq. (6). The Womersley number

conveys in fact a kinetic concept and is an expression of the ratio of inertial forces to viscous forces. The Womersley number is here greater than 1, i. e. that the inertial forces dominate the viscous forces and the velocity function is also not parabolic.

Examining the CSF pressure

Figure 10 shows the distribution of the pressure exerted on brain tissue. The presented numbers have been obtained from ADINA software and indicate the distribution of the pressure exerted by CSF on the walls of brain tissue. When the exerted pressure of CSF on the internal wall of the brain tissue in lateral ventricles increases relative to the pressure exerted by CSF on the internal wall of the brain tissue in subarachnoid space, the pressure gradient is reversed and this leads to change of slope and occurrence of relative extremum in the diagram of figure 11. The effect of brain tissue deformation under CSF loading was examined after extraction of pressure and velocity results. The results show that the maximum deformation of brain tissue is 2.3 mm and occurs in Sylvius aqueduct which has the minimum cross section and maximum pressure.

The brain tissue, as explained in section 3, was considered as a linearly elastic material and the exerted stress on the brain tissue which is also the cause of strain in this tissue, results from the body traction created by CSF in brain tissue. The Poisson's ratio is here constant since the brain tissue was assumed to be homogenous and isotropic. As both Poisson's ratio and module of elasticity are constant in brain tissue, the stress is, based on the linear relationship between stress and strain, proportional to strain and consequently to deformation. Therefore, the deformation reaches exactly there to its maximum value, where the stress is maximum; this has occurred in Sylvius aqueduct.

Figure 11 shows that the maximum and minimum pressure exerted on the brain tissue are 616.3 Pa and 534.8 Pa, respectively. The evaluation results of the exerted pressure on brain tissue are a great help to find a numerical index for assessing the conditions of patients suffering from increased intracranial pressure, hydrocephalus or microcephaly. Based on previous studies, the maximum pressure exerted by CSF aqueduct are 616.3 and 534.8 Pa, respectively.

On the wall of brain tissue is at least 1300 Pa in patients suffering from obstructive hydrocephalus and 2400 Pa in patients suffering from communicating hydrocephalus[27]. As the results show, the range of the pressure exerted by CSF on the brain tissue is very wide in these types of diseases and that makes the use of the maximum pressure as an index to assess the disease difficult. The transmantle pressure gradient, which is the difference between CSF pressure in upper convexity of subarachnoid space and intraventricular space, is also according to previous results no proper index for diagnostic assessment[28]. Thus, a more effective and accurate index to assess the conditions of CSF was introduced in the present study for the first time. This index is the difference between the maximum and minimum pressure exerted by CSF on the walls of cerebral ventricular system. The results obtained from figure 11 were used to compare this pressure difference in Sylvius aqueduct.

The difference between maximum and minimum pressure was used as an index for comparison and assessment since diseases like increased intracranial pressure, hydrocephalus or microcephaly result from changes of CSF pressure on the flow path walls, especially hydrocephalus and microcephaly are caused by pressure changes in ventricular system. As seen in figure 11, the difference between maximum and minimum CSF pressure on the walls of ventricular system equals to 81.5 Pa which is 13% greater than the value calculated by Sweetman. Part of this disagreement is due to the dissimilarity of the cross sections investigated by the two studies. However, the change patterns of these indices relative to each other were similar in both of them. The pressure difference in communicating hydrocephalus is 138 Pa according to previous studies[21]. This be speaks a 70% increase in pressure difference and indicates that the afore-mentioned pressure difference can be a more effective index for assessing this type of diseases[21].

Further, the maximum amount of CSF pressure in the subject under test was measured using lumbar puncture (LP) approach, which was 4.5 mmHg. This amount was 2.6% less than the pressure calculated in this study. This difference is partly due to the conditions of LP test and partly due to the reason that the pressure obtained by LP approach equals almost to ICP. The transmantle pressure gradient is 4 Pa according to reports of previous studies, so there should be the same difference between the calculated pressure in this study and the pressure obtained from LP[21].

Due to limitations of pressure gauge, it wasn't possible to extract the difference between the maximum and minimum CSF pressure through LP approach in this study, but as mentioned before, the result of the maximum pressure comparison indicates an acceptable agreement between the pressure obtained by LP and the pressure calculated in this study. So utilizing a digital pressure

gauge with proper sensitivity in LP approach to measure the difference between maximum and minimum pressure, makes it possible to use this difference, alongside with the results of this study, to assess the CSF pressure conditions in analysis of diseases.

CONCLUSIONS

Through a 3D assessment of the cerebral ventricular system using FSI approach, it was shown in this study that the difference between the maximum and minimum pressure exerted by CSF on the brain tissue in Sylvius aqueduct is a reliable index to explore and evaluate the CSF conditions and this index can be used in diagnosis of diseases like hydrocephalus and microcephaly or the type of diseases resulting from Increased ICP. Moreover, the possibility of practical application of the results of this study was demonstrated by comparing the calculated CSF pressure values and the CSF pressure data obtained from LP test.

ACKNOWLEDGMENTS

The team of authors appreciates and values the efforts of Dr. Rahimianin for providing PC-MRI data and Mrs Banooashraf Saberi and Mr. Esmail Seddighi for their great participation in the data analysis and editing this manuscript.

REFERENCES

1. Nolte J, Sundsten W. The Human Brain: An Introduction to its Functional Anatomy, fifth ed, Mosby, Stlouis; 2002.
2. Guyton AC, Hall JE. Textbook of Medical Physiology; 2006.
3. Nolte J. The human brain: an introduction to its functional anatomy. Mosby-Year Book, Inc, issouri; 1993.
4. Fenis H, Dauber W. Pocket atlas of human anatomy. 5thed; 2007.
5. Nagashima T, Tamaki, N, Matsumoto S, Horwitz B, Seguchi Y. Biomechanics of hydrocephalus: a new theoretical model. Jounal of Neurosurgery. 1987;21(6):898–904.
6. Miller K. Constitutive model of brain tissue suitable for finite element analysis of surgical procedures. Journal of Biomechanics. 1999;32:531–537.
7. Min Liu. A Tree Dimentional hyperviscoelastisity model for the dynamic response, Msc. Thesis, University akro Akron; 2007.
8. Chafi GG, Chandra N. Dynamic Response Brain Subjected Blast Loadings: Influence of Frequency Ranges, Journal of Applied Mechanics. 2011:3:803–823.
9. Taylor Z, Miller K. Reassessment of brain elasticity for analysis of Biomechanisms of hydrocePhallus, Journal of Biomechanics. 2004;37:1263–1269.
10. Milhorat TH, Chou MW, Trinidad EM, Kula RW, Mandell M, Wolpert C, et al. Chiari Imalformation redefined: clinical and radiographic findings for 364 symptomatic patients. Neurosurgery. 1999;44:1005–1017.
11. Fin L, Grebe R. Three dimensional modeling of the cerebrospinal fluid dynamics and brain interactions in the aqueduct of sylvius, Comput. Method. Biomech. 2003;6:163–170.
12. Kurtcuoglu V, Soellinger MP, Summers K, Boomsma D, Poulikakos P, Boesiger Y, et al. Computational investigation of subject-pecific cerebrospinal fluid flow in the third ventricle and sylvius Aqueduct, Journal of Biomechanic. 2007;40:1235–1245.
13. Cheng S, Tan K, Bilston LE. The effects of the interthalamic adhesion position on cerebrospinal fluid dynamics in the cerebral ventricles. J Biomech. 2010;43:579–582.
14. Jacobson EE, Fletcher DF, Morgan MK, Johnston IH. Computer modelling of thecerebrospinal fluid flow dynamics of aqueduct stenosis. Med Biol Eng Comput. 1999;37:59–63.
15. Jacobson EE, Fletcher DF, Morgan MK, Johnston IH. Fluid dynamics of the cerebral aqueduct, Pediatr. Neurosurg. 1996;24:229–236.
16. Linge SO, Haughton V, Lovgren AE, Mardal KA, Langtangen HP. CSF flow dynamics at the craniovertebral junction studied with an idealized model of the subarachnoid space and computational flow analysis. AJNR Am J Neuroradiol. 2010;31:185–192.
17. Gupta S, Soellinger M, Boesiger P, Poulikakos D, Kurtcuoglu V. Three- dimensional computational modeling of subject-specific cerebrospinal fluid flow in the subarachnoid space, J. Biomech. Eng. 2009;131:1–11.
18. Özkan Ü, Alp K, Avcu S, Etlik Ö, Arslan H, et al. Phase-contrast MRI evaluation of normal aqueductal cerebrospinal fluid flow according to sex and age. J Diagn Interv Radiol. 2009;15:227–231.
19. Yu Q, Kong X, Liu D. Differential diagnosis of arachnoid cyst from subarachnoid space enlargement by Cine - Phase - contrast cine MRI. CMJ. 2003;116(1):116 -120.
20. Zhu DC, Xenos MAA, Linniger, Penn RD. Dynamics of Lateral Ventricle and Cerebrospinal Fluid in Normal and Hydrocephalic Brains. J Magn Reson Imaging. 2006;24(4):756-70.
21. Sweetman B, Xenos M, Zitella L, Linniger AA. Three-dimensional computational prediction cerebrospinal fluid flow in the human brain, Journal of Computers in Biology and Medicine. 2011;41:67–75
22. Linniger AA, Sweetman B, Penn R. Normal and hydrocephalic brain dynamics:the role of reduced celebrospinal fluid reabsorption in entricular enlagment. Annals of biomechanic eng. 2009;37:1434-1447.
23. Segal MB. Transport of nutrients across the choroid plexus. Microsc Res Tech. 2001;52:38–48.
24. Linninger AA, Xenos M, Zhu DC, Somayaji MR, Kondapalli S, Penn RD. Cerebrospinal fluid flow in the normal and hydrocephalic human brain. IEEE Trans Biomed Eng. 2007;54(2):291-302.

25. ADINA R&D, Inc, Theory and Modeling Guide, Volume I and III: ADINA and ADINA-F; 2008.

26. Bonet J, Marriott H, Hassan O. An averaged nodal deformation gradient linear tetrahedral element for large strain explicit dynamic applications, Commun Number. Methods Eng. 2001;17:551–561.

27. Joel A. Lefever, José JG, Joshua H. Smith, A patient-specific, finite element model for noncommunicating hydrocephalus capable of large deformation, Journal of Biomechanics. Online publication date: 1-Apr-2013.

28. Stephensen H, Tisell M, Wikkelsö C. There is no transmantle pressure gradient in communicating or non communicating hydrocephalus. Neurosurgery. 2002;50:763–773.